Nyquist-WDM filter shaping with a high-resolution colorless photonic spectral processor

David Sinefeld,[1,*] Shalva Ben-Ezra,[2] and Dan M. Marom[1]

[1]*Applied Physics Department, Hebrew University, Jerusalem 91904, Israel*

[2]*Finisar Corporation, Nes Ziona, Israel*

**Corresponding author: sinefeld@gmail.com*

Received May 8, 2013; revised July 26, 2013; accepted July 29, 2013;
posted July 30, 2013 (Doc. ID 190284); published August 21, 2013

We employ a spatial-light-modulator-based colorless photonic spectral processor with a spectral addressability of 100 MHz along 100 GHz bandwidth, for multichannel, high-resolution reshaping of Gaussian channel response to square-like shape, compatible with Nyquist WDM requirements. © 2013 Optical Society of America

OCIS codes: (060.2330) Fiber optics communications; (130.7408) Wavelength filtering devices.
http://dx.doi.org/10.1364/OL.38.003268

High-spectral-efficiency modulation formats and dense packing of wavelength division multiplexing (WDM) channels are key techniques for maximizing the transmission capacity over the available optical gain window. Two different approaches are actively being investigated for placing the signals at the packing limit, when the baud rate equals the channel spacing: coherent optical orthogonal frequency-division multiplexing (CO-OFDM) and Nyquist WDM (N-WDM). In CO-OFDM, the subcarriers are synchronously modulated with rectangular pulses in time, creating sinc-like spectra. The modulation rate equals the carrier separation such that the sinc nulls fall on neighboring carriers. While the spectral components of neighboring channels overlap, channel crosstalk can be averted by proper filtering and signal processing (SP) at the receivers. In N-WDM, the signal is modulated with sinc pulses in time, suggesting strong intersymbol interference (ISI) due to overlapping neighboring pulses. By receiver sampling at the sinc peak position, ISI can be avoided due to the constant zero spacing property of the sinc function. The square-like spectral form of N-WDM is amenable to nonoverlapping and contiguous packing. N-WDM and CO-OFDM can be seen as complementary schemes, overlapping in either the time or frequency domain. In theory, both modulation formats can reach the same sensitivity performance; however, in practical scenarios, N-WDM requires less receiver bandwidth (due to its limited spectral extent) and slower analog-to-digital converters [1]. These formats support the construction of terabit superchannels that propagate between endpoints with no intermediate filtering elements [2,3].

Both CO-OFDM and N-WDM require careful control over the modulated signal form, to reach their desired attributes. This can be obtained by electrically shaping the modulator driving signals through transmitter digital SP circuitry and digital-to-analog converters [4,5]. However, the electrical SP tasks are both power-consuming and costly. Alternatively, all-optical techniques have been proposed, which are based on passive filtering arrangements, which are further not rate limited to electronic SP abilities. OFDM receivers and transmitters [6–9] have been realized through interference-based devices. N-WDM transmission experiments [10–13] typically employ filters originally designed for channel add–drop. As such their performance attributes fall short of those required to optimally support N-WDM.

In this Letter, we capitalize on the high-resolution filtering attributes of a photonic spectral processor (PSP), which is an enhanced version of our former device [14], and use it in cascade with a multiplexing filter having Gaussian passband characteristics (see Fig. 1). We adjust the PSP for spectral reshaping to generate a square-like spectrum, conforming to the N-WDM requirements.

The key to the fine optical resolution of our PSP is its operation over a small free spectral range (FSR), in this case 100 GHz. The dispersive medium is an arrayed waveguide grating (AWG) planar lightwave circuit (PLC), having 34 grating arms fabricated in silica-on-silicon technology with 0.8% index contrast. The output of the AWG is unconventional: instead of employing a second slab-lens region that demultiplexes to output waveguides, the grating arms terminate at the PLC edge at fixed pitch, and the light radiates normally into free space. This forms a phased-array output that experiences angular dispersion on account of wavelength-dependent phase delays. An $f = 3$ mm cylindrical lens that is affixed at

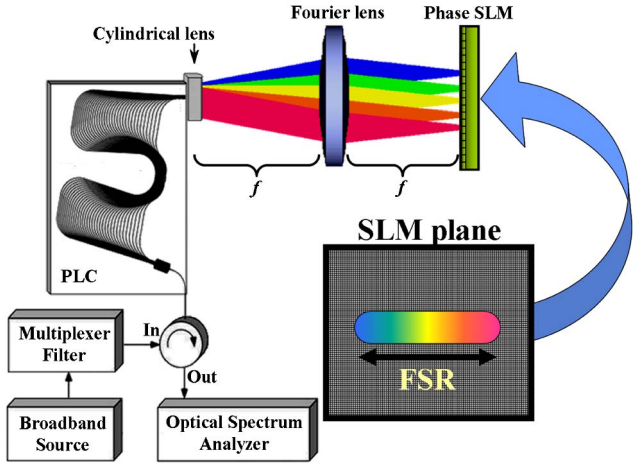

Fig. 1. Experimental layout making use of the PSP for shaping to a rectangular spectrum with the liquid crystal on silicon (LCoS) spatial light modulator (SLM). The SLM applies linear phase tilts to each spectral component for encoding coupling losses to the desired spectral shape.

the PLC edge collimates the light in the guided direction. The optical resolution of the AWG is the FSR divided by the waveguide arm count, resulting in ~3 GHz spectral resolution. The same resolution can be obtained with an AWG having larger FSR, but would require a larger waveguide count (and larger AWG device layout). Likewise, we can obtain finer resolution with the same FSR if we increase the waveguide count (again at the expense of a larger AWG). For our purposes here, the 3 GHz suffices to demonstrate the square filtering function.

The angularly dispersed output radiated light is projected with a Fourier lens using a simple f-f arrangement onto a liquid crystal on silicon (LCoS,) two-dimensional phase spatial light modulator (SLM) that is controlled by a computer. The resulting PSP is therefore a hybrid guided-wave/free-space optics device. The reflective LCoS SLM is placed at the Fourier plane, where the spectral components of the incident optical signal are spatially dispersed and manipulated. This arrangement yields a flat spectral response over the entire FSR, in contrast to our previous PSP implementation [14], where the grating arms terminated in a slab lens and then radiated into free space. This required a complicated telescopic free-space arrangement, which experienced spectral apodization. Due to the periodic nature of the dispersion (originating from the FSR property of the AWG), spectral elements that are shifted by FSR multiples overlap in space and the same channel response is achieved every FSR (the colorless property, when the FSR equals the channel separation).

The required square-like spectral filter response in N-WDM is the cumulative transfer function of the multiplexing components. Hence, we need to take into account the response of the multiplexer, typically of Gaussian shape. A typical optical N-WDM implementation would thus separately multiplex the even and odd channels, shape each group to square-like channel response with a 50% spectral duty cycle, and passively combine the two interleaved halves (Fig. 2).

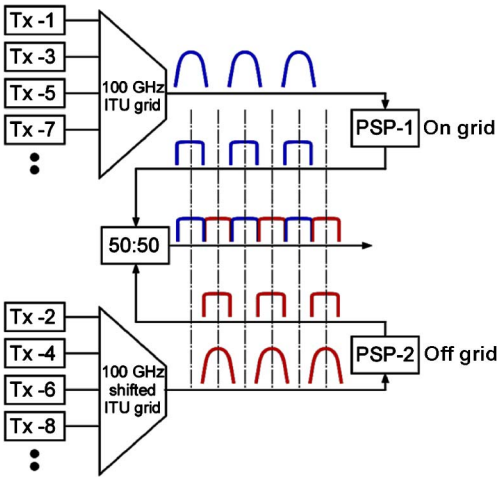

Fig. 2. Proposed method for generating a Nyquist-WDM superchannel: odd square channels (marked in blue) are generated using an on-grid PSP filtering the output of a 100 GHz ITU grid demultiplexer, while even square channels (marked in red) are generated using an off-grid PSP filtering the output of a 100 GHz shifted ITU grid demultiplexer.

The PSP needs to flatten the spectral response of the multiplexer, by imparting excess loss to the central spectral components, such that their magnitude equates the edge spectral components. In our specific example making use of a 100 GHz spaced PSP, two 100 GHz spaced multiplexers are utilized, one for multiplexing the odd channels (*on-grid*) and the other for the even channels (*off-grid*). Each set is then spectrally shaped using a PSP to a square spectrum of 50 GHz bandwidth, and the two interleaving signal components are passively combined. For such scenarios, the colorless property of the PSP is ideally suited, as the PSP imparts the same response to multiple channels simultaneously at high resolution.

The elements of the PSP, consisting of the AWG PLC, an $f = 100$ mm Fourier lens, and the LCoS phase SLM, were assembled on an optical table. A circulator was used to separate the input and output light to the PLC. We used Holoeye PLUTO LCoS SLM that has 1920×1080 pixels of 8 μm pitch, with a system spatial dispersion of $dx/d\lambda = 10$ [mm/nm], which translates to 100 MHz shift in center frequency per SLM column. The entire 100 GHz spectrum spans over 1000 columns. The insertion loss of the PSP is 15 dB, caused mostly by excessive AWG losses (~12.5 dB) and SLM losses (~2.5 dB).

For the N-WDM filtering application, the 100 MHz addressability dictates the precision at which the filter bandwidth can be set, and the 3 GHz resolution sets the roll-off shape (deviation from ideal square-like filter response). This is experimentally shown in Fig. 3, where the filter edge is displaced in increments as fine as 100 MHz. The roll-off shape is always maintained, and determined by the spectral resolution, regardless of the filter bandwidth, with a decrease from −0.5 to −10 dB (equivalent to a 90-10 fall) in 5 GHz bandwidth.

In order to amplitude modulate the dispersed spectral components with a phase-only LCoS SLM, we use the direction orthogonal to the dispersion to locally manipulate the reflected beam. To prescribe amplitude modulation, we apply a phase tilt, on a column-by-column basis, that introduces a coupling loss back into the AWG for each spectral component, subject to the optical resolution constraint.

In order to generate filtering for both on/off grid channels with the same PSP, a flat spectral response is required, as experimentally achieved (dashed-purple line

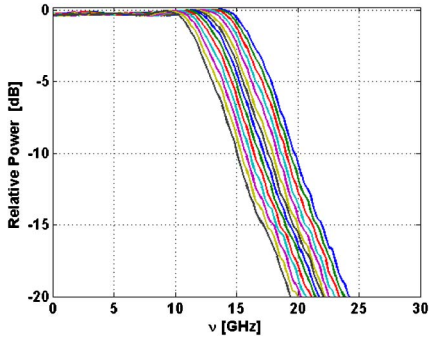

Fig. 3. Experimental results of PSP filter width change, one column at a time. For each position, 10 dB attenuation is reached at less than 5 GHz bandwidth. Although the system has 100 MHz addressability, the filter edge position is shifted here in 400 MHz increments for clarity only.

in Fig. 4). As a first demonstration of the flattening abilities of the PSP, we used an etalon-based tunable spectral filter with a Lorentzian line shape that was placed after an amplified spontaneous emission source. The filter response is plotted in Fig. 4 as a dashed-black line. The PSP was placed afterward, and flattened the spectral response by applying an inverse attenuation function over prescribed bandwidths. In this fashion, we show square-like spectral response for 30, 40, and 50 GHz bandwidths with <0.5 dB ripple [Fig. 4(a)]. As we prescribe larger bandwidths, the overall filter attenuation at the center must be increased [see Fig. 4(b)] in order to achieve flat equalization over the bandwidth target.

The temporal response of the flattened spectrum was characterized by filtering ultrashort pulses (100 fs) emitted from a Spectra Physics Tsunami+Opal mode locked laser ($\lambda = 1.55$ μm, 80 MHz rate). The laser output was fiber coupled and traversed the etalon filter and the PSP, allowing transmission of the single flattened channel only. With the PSP, we applied the same cascaded spectral responses that were measured and shown in Fig. 4(a). The temporal response of 30, 40, and 50 GHz channel bandwidths was measured using a high-speed sampling (HSS) scope, resulting in sinc^2 shaped intensity pulses with widths of 33, 25, and 20 ps, respectively (Fig. 5). A comparison to the expected sinc^2 functions shows an excellent match to the measured results.

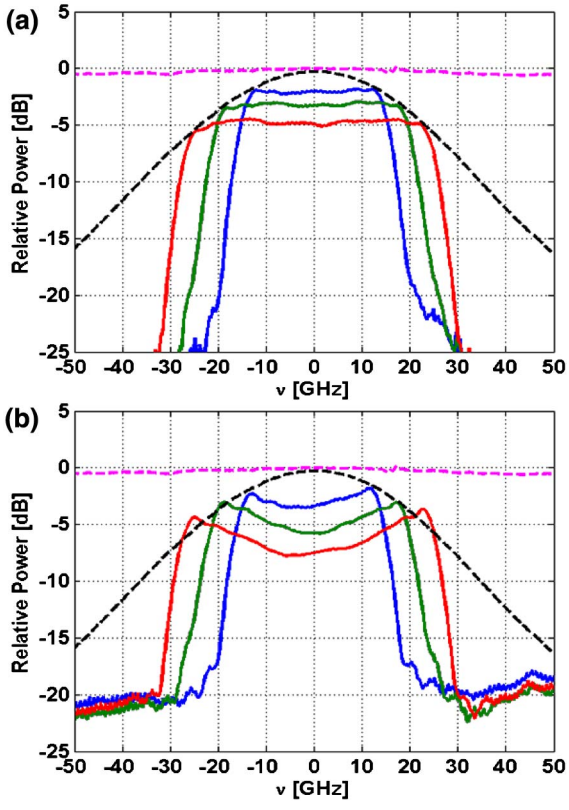

Fig. 4. Experimental results of rectangular spectral filter response, compensating a commercial multiplexing filter (marked with dashed-black line) for three selected bandwidths: 30, 40, and 50 GHz. (a) Cascaded flattened spectrum for three bandwidths. As the bandwidth becomes larger, overall filter attenuation must be increased in order to achieve equalization. (b) Encoded PSP response without the multiplexer [different colors match those of (a)]. The dashed-purple line denotes the PSP response without any spectral shaping, showing a flat response along the entire usable bandwidth.

Our N-WDM solution is based on the colorless property of the PSP, and would operate simultaneously for all WDM channels spaced at FSR. In order to demonstrate this ability, a combination of flattened 50 GHz on-grid and off-grid channels is needed. Although two different 100 GHz multiplexers are required (on and off grid), it is still desirable to use identical PSP in both channel sets. The PSP AWG is designed with 100 GHz FSR aligned for on-grid operations. When placed in cascade with an on-grid multiplexer, the central 50 GHz are flattened by applying varying tilted phases with the LCoS SLM, and a large constant phase tilt outside the central band for high attenuation [Fig. 6(a)]. For off-grid channel flattening, the outer parts of the FSR are shaped using the varying tilted phase, where the central part is blocked by the large attenuation [Fig 6(b)]. This demonstrates the coherent combining of frequency components separated to two different diffraction orders at the FSR edge. The PSP spectral response is shown in Figs. 6(c) and 6(d), showing the desired 50 GHz inverse correction function for both (on/off grid) channel sets.

In order to demonstrate optical N-WDM channel filtering, we used a Finisar WaveShaper (1000S) to simulate multiplexed Gaussian WDM channel spectra both on-grid [Fig. 6(e)] and off-grid [Fig. 6(f)]. Both multiplexer responses were compensated by the PSP functions introduced in Figs. 6(b) and 6(d), resulting in rectangular spectral shaping having 50% duty cycle [Figs. 6(g) and 6(h)]. The two branches can then be passively combined, resulting in the entire spectrum being occupied with no spectral gaps and <1 dB ripple [Fig 6(i)].

The filtering abilities of the high-resolution PSP that were demonstrated here can be the key for better utilization of the available communication spectrum by better conforming to the N-WDM format. The high-resolution PSP can also support more aggressive time-frequency packing formats that do allow controlled amounts of either channel crosstalk or ISI with excess channel coding

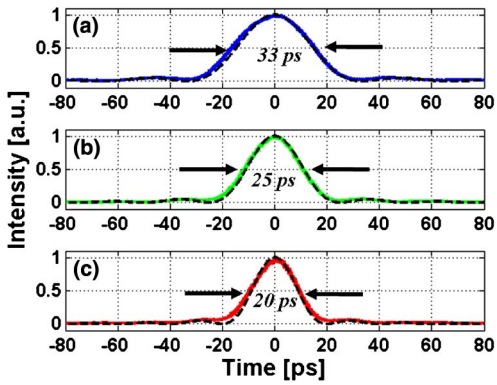

Fig. 5. Time-domain measurements of (a) 30 GHz, (b) 40 GHz, and (c) 50 GHz carved spectra, resulting in 33, 25, and 20 ps width sinc^2 shaped pulse intensities, respectively, measured with a high-speed sampling scope. The measured temporal results are plotted as solid color lines, matching the bandwidth filters of Fig. 4. Expected sinc^2 functions with the desired widths are plotted as dashed black lines, showing an excellent match to the measured results.

for error-free signal recovery [15]. We also demonstrated on/off grid flattening abilities, which enable the use of identical PSP devices for a complete N-WDM system.

The loss contributions of the AWG (~12.5 dB) are caused mostly by fabrication errors and can be overcome by a phase error correction mechanism [16], to allow future application in an actual N-WDM network. Although system losses are worse than in a state-of-the-art waveshaper (typical insertion loss of –5 dB), our PSP resolution of 3 GHz is at least twice as good [11]. We should note that temperature changes of the system result in a spatial shift in the dispersed spectrum. This can be compensated by tracking the LCoS filter spectral position and actively compensating for the thermal shift in the passband position.

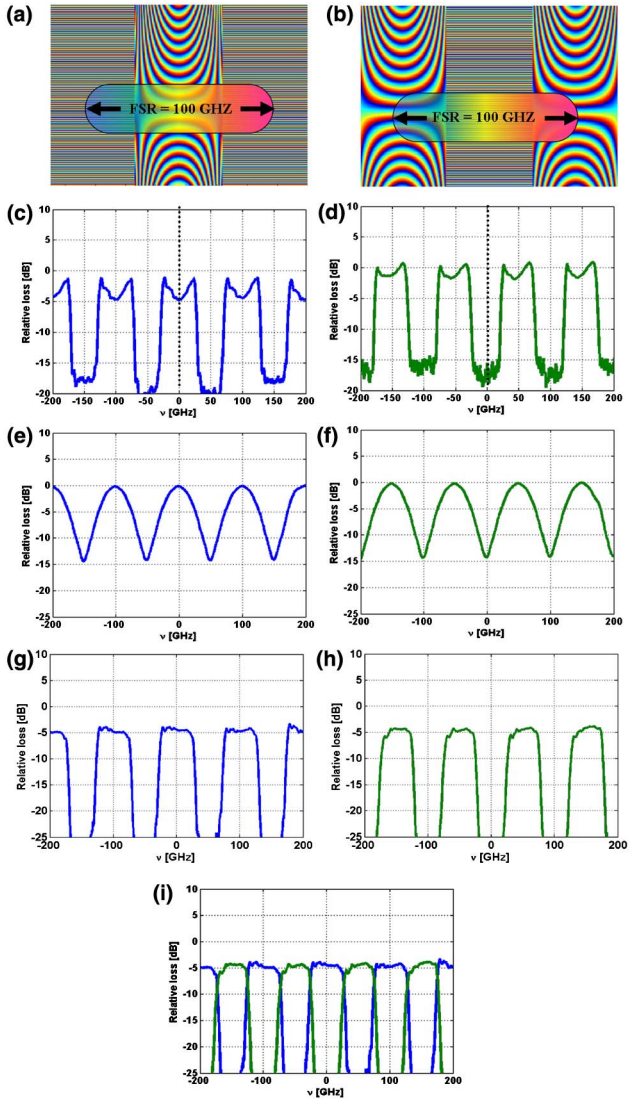

Fig. 6. Experimental demonstration of optical N-WDM filtering. (a) SLM pattern for on-grid channel filtering with varying phase tilts along the central 50 GHz and large constant phase tilt outside, and (b) SLM pattern for the off-grid channel filtering with varying phase tilts along the outer 50 GHz and large constant phase tilt along the center. Resulting (c) on-grid and (d) off-grid PSP spectral response. (e) On-grid and (f) off-grid Gaussian response of multiplexer, simulated with Finisar WaveShaper. Cascaded spectral filtering response for (g) on-grid and (h) off-grid, yielding interlaced rectangular shaped channels with 50% duty cycle. (i) Passively combined on-grid and off-grid components of each branch, resulting in full spectral coverage with <1 dB ripple.

The authors thank the Israel Ministry of Industry and Trade TeraSanta program and EC FP7 ICT FOX-C and OTONES programs for funding.

References

1. G. Bosco, A. Carena, V. Curri, P. Poggiolini, and F. Forghieri, IEEE Photon. Technol. Lett. **22**, 1129 (2010).
2. Y. Ma, Q. Yang, Y. Tang, S. Chen, and W. Shieh, Opt. Express **17**, 9421 (2009).
3. G. Bosco, V. Curri, A. Carena, P. Poggiolini, and F. Forghieri, J. Lightwave Technol. **29**, 53 (2011).
4. X. Zhou, L. Nelson, P. Magill, B. Zhu, and D. Peckham, in *Optical Fiber Communications Conference*, OSA Technical Digest (Optical Society of America, 2011), paper PDPB3.
5. R. Schmogrow, M. Winter, M. Meyer, D. Hillerkuss, S. Wolf, B. Baeuerle, A. Ludwig, B. Nebendahl, S. Ben-Ezra, J. Meyer, M. Dreschmann, M. Huebner, J. Becker, C. Koos, W. Freude, and J. Leuthold, Opt. Express **20**, 317 (2012).
6. D. Hillerkuss, M. Winter, M. Teschke, A. Marculescu, J. Li, G. Sigurdsson, K. Worms, S. Ben Ezra, N. Narkiss, W. Freude, and J. Leuthold, Opt. Express **18**, 9324 (2010).
7. K. Lee, C. T. D. Thai, and J.-K. K. Rhee, Opt. Express **16**, 4023 (2008).
8. Z. Wang, K. S. Kravtsov, Y.-K. Huang, and P. R. Prucnal, Opt. Express **19**, 4501 (2011).
9. A. J. Lowery and L. Du, Opt. Express **19**, 15696 (2011).
10. G. Gavioli, E. Torrengo, G. Bosco, A. Carena, S. Savory, F. Forghieri, and P. Poggiolini, IEEE Photon. Technol. Lett. **22**, 1419 (2010).
11. R. Cigliutti, E. Torrengo, G. Bosco, N. P. Caponio, A. Carena, V. Curri, P. Poggiolini, Y. Yamamoto, T. Sasaki, and F. Forghieri, J. Lightwave Technol. **29**, 2310 (2011).
12. Z. Dong, J. Yu, H. Chien, N. Chi, L. Chen, and G. Chang, Opt. Express **19**, 11100 (2011).
13. M. Nakazawa, T. Hirooka, P. Ruan, and P. Guan, Opt. Express **20**, 1129 (2012).
14. D. Sinefeld and D. M. Marom, IEEE Photon. Technol. Lett. **22**, 510 (2010).
15. N. Sambo, F. Paolucci, F. Cugini, M. Secondini, L. Poti, G. Berrettini, G. Meloni, F. Fresi, G. Bottari, and P. Castoldi, in *Optical Fiber Communications Conference*, OSA Technical Digest (Optical Society of America, 2013), paper OTh1H.5.
16. D. Sinefeld, N. Goldshtein, R. Zektzer, N. Gorbatov, M. Tur, and D. M. Marom, in *Advanced Photonics Congress*, OSA Technical Digest (Optical Society of America, 2012), paper JTu5A.55.